Measurement of near-wall 3D flow velocity from wave-guiding micro-pillars

CHRISTOPH BRUECKER

School of Mathematics, Computer Science and Engineering, Department of Mechanical Engineering and Aeronautics, City University London, Northampton Square , London DC 20036, United Kingdom
christoph.bruecker@city.ac.uk

Abstract: The measurement of near-wall flow in a plane close to the wall is achieved using the wave-guiding feature of transparent flexible micro-pillars which are attached in a 2D array to a surface and bend with the flow. Optical detection of bending from below the surface and application of auto-correlation methods provide mean and fluctuating part of the components of the wall-parallel velocity components. In addition, the wall-normal fluid motion is determined from spatial gradients in the array. The data provide the three-component velocity vector field in a plane close to the wall as well as their statistics.

OCIS Codes: (110.2350) General; (280.7250) General Science.

References

1. M. Raffel, C. Willert, S. Werley, J. Kompenhans, *Particle Image Velocimetry PIV: a practical guide* (Springer 2007).
2. C. Brücker C, J. Spatz, W. Schroeder, "Feasibility study of wall shear stress imaging using micro-structured surfaces with flexible micro-pillars," Exp. Fluids **39**, 464–474 (2005).
3. C. Brücker, "Evidence of rare backflow and skin-friction critical points in near-wall turbulence using micropillar imaging," Phys. Fluids **27**, 031705 (2015).
4. J. Paek, J. Kim, "Microsphere-assisted fabrication of high aspect-ratio elastomeric micropillars and waveguides," Nature Communications **5**, 3324 (2014).
5. C. Skupsch, T. Klotz, H. Chaves, C. Brücker "Channeling optics for high quality imaging of sensory hair," Rev. Sci. Instrum. **83**, 045001K (2012).
6. C. Brücker, R. Wagner, M. Köhler " Measurements of wall-shear stress fields on the piston crown in an IC engine flow using fluorescent labelled micro-pillar imaging," Proc. 18th Int. Symp Appl. Laser Techniques to Fluid Mechanics, Lisbon, (2016).
7. A.M. Gambaruto, D.J. Doorley, T. Yamaguchi, "Wall shear stress and near wall convective transport. Comparisons with vascular remodeling in a peripheral graft anasthomosis," J. Comp. Physics **229** (14), 5339-5356 (2010).
8. S. Scharnowski, R.Hain, C. J. Kähler " Estimation of Reynolds Stresses from PIV Measurements with Single-Pixel Resolution," Proc. 15th Int. Symp. Appl. Laser Techniques to Fluid Mechanics, Lisbon, (2010).

1. Introduction

The velocity field next to the surface of a body is of high importance for momentum and heat transfer, sediment transport and mixing. Pointwise measurements using hot-wires are nowadays standard in fluid mechanics, they can provide details of the local flow fluctuations down to distances of about 100-500µm from the wall. Laser-based methods such as Laser-Doppler Anemometry (LDA) or Particle-Image-Velocimetry (PIV) require the addition of small tracer-particles that scatter the light and follow the flow with negligible slip [1]. Applications of these methods near walls require dense seeding of the flow near the wall which is a challenge in many wind-tunnel flows [1]. In addition, reflections at the wall and particles adhering to the wall deteriorate the signal processing. Due to the high shear in the boundary layer the particles are also subject to lift forces, limiting the data rate.

In 2005, the method of micro-pillar wall-shear stress imaging was developed [2] which is a tracer-less method to investigate the wall-shear stress (WSS) distribution. Recent studies in a turbulent boundary layer flow at zero pressure gradient could provide for the first time evidence

of critical points in the WSS field and the existence of rare backflow events using this method [3]. Processing of the data to obtain the tip displacement in the images required template matching and recording of reference markers which limited the accuracy of tip deflection measurement.

Herein, micro-pillar imaging is done with a camera from below the bottom of the micro-pillars taking advantage of the wave-guide properties of the transparent flexible micro-pillars. Their tips are fluorescent labelled to improve the signal to noise ratio of the wave-guiding signal. This allows applying correlation methods to process the WSS field and statistics of it. Finally, use of the fundamental equations of fluid mechanics offers to determine the wall-parallel velocity components and the wall-normal one, too. Thus, all three velocity components can be determined in a wall-parallel plane close to the wall. The method is described in section 2 and exemplary measurements on a flat plane of a piston crown in intake flow conditions are shown in section 3. In section 4 results are discussed and conclusions are drawn.

2. Method

The basic principle of micro-pillar WSS imaging is to capture the displacement of the micro-pillar tips relative to their position in unforced situation (no flow). This measure can be related to the local WSS after calibration [2]. The bending of the flexible hair-like structures in flow relative to their unforced situation (no-flow) is usually recorded in submicron resolution in direct view of the tip. Since the material of the pillars we use is a transparent elastomer (PDMS), the pillars in principle offer wave-guiding features. The schematic concept is given in Fig. 1.

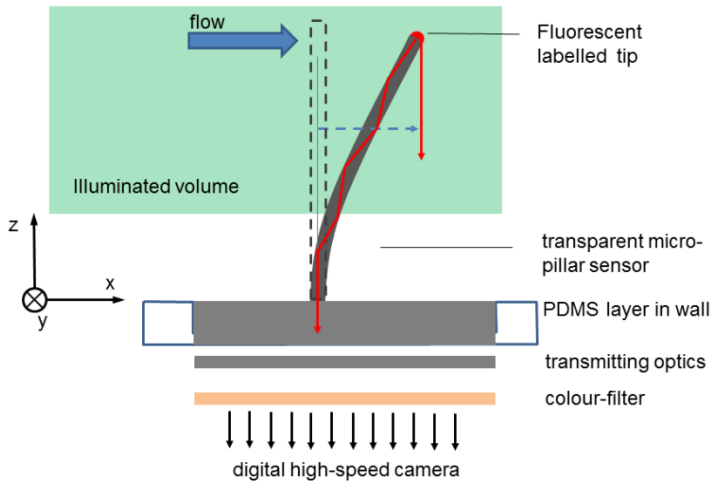

Fig. 1. Set-up of the subcutaneous recording of the pillar tip deflection using fluorescent labelled tips of the transparent pillars and their wave-guidance properties. The blue arrow indicates the relevant measure of tip displacement ***Q*** relative to the no-flow situation that is captured by the imaging system below the wall.

The wave-guiding feature of the micro-pillars has been noted already in the original publication [2] and has recently been re-stated in [4]. When light is scattered from a source location at the tip of the fiber in an environment of lower refractive index, the light is guided through the fiber towards the footage. Herein, we use a labelling technique with fluorophores on the tip of the pillars and illuminate those with laser light in the corresponding excitation wavelength.

2.1 Micro-pillar array

The reproducible and homogeneous circular shape of the micro-pillars achieved in our manufacturing process is important to get good optical properties of this wave-guidance effect. The micro-pillars used in this work are displayed in Fig. 2. They are made from polydimethylsiloxane (PDMS, ρ =1050 kg/m3, Young's modulus E≈1.76×10^6 N/m^2), L = 390 µm long and d = 20µm in diameter [5]. Therefore we used deep etching of a silicon wafer to generate a mold form which is filled with PDMS. After curing the transparent layer with the micro-pillars is peeled-off [5]. A typical two-dimensional array consists of 30 × 30 micro-pillars with an interspacing of 500µm in a quadratic array. Such an array has been used in previous measurements [5] and has shown good resolution in spatial and temporal response of the micro-pillar array for measurements in turbulent flows. The interspacing is > 20 times the pillar's diameter which ensures that there is no interference of the response of neighboring micro-pillars. On the other hand the interspacing is small enough to capture even the smallest scales in the flow.

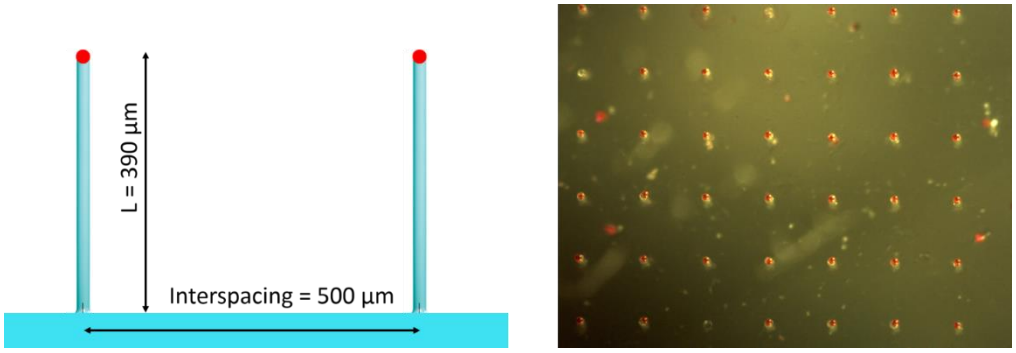

Fig. 2. Sketch of the fluorescent labelled pillar tips (left) and picture as seen from top onto the regular array mounted as an insert in a flat transparent plate (right).

The labelling of the tips was achieved by stamping the array bottom up into a thin layer of PDMS mixed with the fluorophore Rhodamine B. The labelling is applied to remove any direct light from the illumination system on the sensor and to improve the signal to noise ratio of the wave guiding signal. The static and dynamic sensor response was investigated with the methods described in [5]. The damped natural frequency of the micro-pillar in water is about $f_{0,D}$ ≈ 1053Hz with $f \leq 0{,}3f_0$ being the application range of the sensor array.

2.2 Imaging from bottom

The above described arrays of fluorescent labelled micro-pillars are on top of the cast which contains also a 2mm tick PDMS base layer for handling and integration of the sensor array into a wall of the investigated boundary layer flow. Such a wall is the piston head in a reciprocating engine, which we took as an example of a complex wall-bounded flow, the set-up is described in detail in [6]. The piston head is a transparent disc made of Perspex (height 20mm, diameter D=78mm) with an insert for the micro-pillar array. The array is positioned such that it is flush with the top wall and the pillars protrude into the flow. Illumination of the pillars is done with

a light-sheet generated by a pulsed Nd:YLF laser (Litron Nd:YLF, 30 mJ at 300 Hz repetition rate, wavelength 527 nm).

The recording was done with a high-speed camera and lens system below the transparent disc. A typical section of the image taken with a high-speed camera (Blue-Cougar-XD104, 1024×499 px, 300fps) after contrast-enhancement highlights a characteristic pattern as shown in Fig. 3. It consists of the direct light spot received from the tip plus an additional spot that originates from the emitted light that is guided through the micro-pillar towards the base. The processing of the images is explained in section 2.4. Note that the contrast enhancement largely exaggerates the spot size and is only done here for reasons of clarity in Fig. 3.

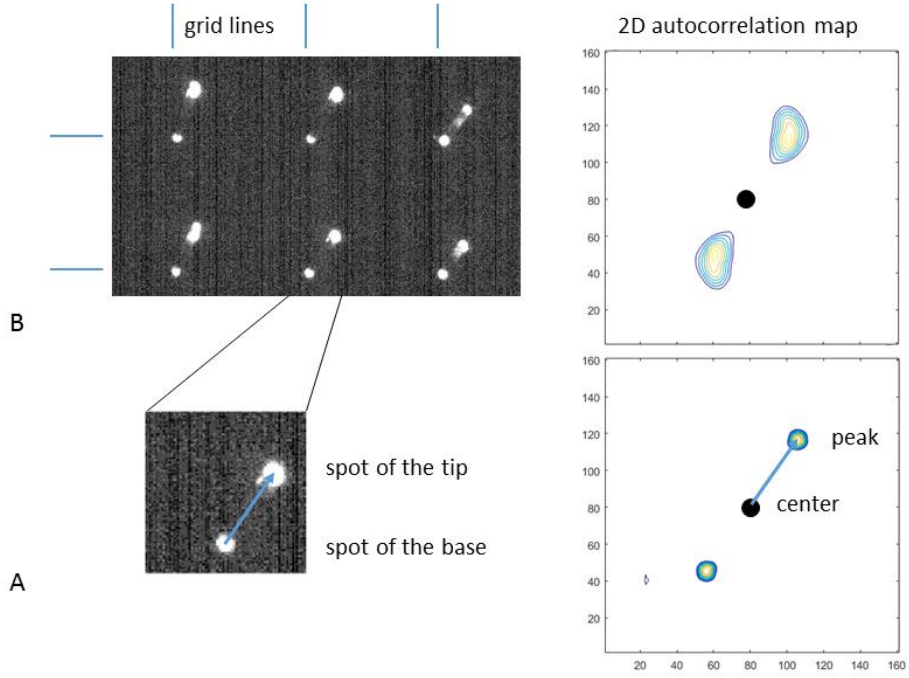

Fig 3: Image after stark contrast enhancement as seen from below the bottom of the transparent wall with the pillars in flow (flow is from bottom to top right). The blue lines indicate the grid of the pillars' base. The image demonstrates that a spot appears at the base and the tip. A: section of one single sensor and corresponding autocorrelation map (right) after subtraction of the central peak; B: section of 3x2 sensor field and corresponding autocorrelation map (right).

2.3 Tip bending information

Measurements of the pillar tip deflection with the subcutaneous recording provide the projection of the end-to-end vector in the wall-parallel x-y-plane $\boldsymbol{Q}$ with its components Qx and Qy. In the image plane it is the offset between the tip spot and the base spot, see Fig. 3. Magnitude and direction of this offset represents the micro-pillar's bending due to the drag forces acting along it imposed by the near-wall flow velocity vector **u**. The tip displacement (magnitude and direction) for small micro-pillars is in first approximation proportional to the two-dimensional wall shear stress vector [2]

$$\boldsymbol{\tau}_W = \mu \left. \frac{\partial \mathbf{u}_\perp}{\partial z} \right|_{z=0} = \boldsymbol{f}\left(\mathbf{Q}\right) \tag{1}$$

where the subscript ⊥ denotes the two horizontal (or tangential) x- and y-components of coordinates along the wall. The constant and any higher order correction terms can be obtained from a calibration procedure in a given shear flow [2]. Skin friction and wall stress fields are defined by velocity derivatives normal to the wall in z-direction. Using a Taylor expansion, the information of the velocity field in a plane close to the wall at a distance z=δn is related to the WSS as follows, see [7]:

$$\mathbf{u}_\perp = 1/\mu \, \boldsymbol{\tau}_W \, \delta_n + O(\delta_n^2) \, . \tag{2}$$

The boundary condition is the non-slip condition at the surface which means a zero velocity relative to the wall at z=δn=0. In addition, the solenoidal fluid condition in incompressible flows allows to determine the wall-normal component of the velocity vector from the divergence of the WSS components [7]:

$$u_n = -\tfrac{1}{2} \mu \, (\nabla \cdot \boldsymbol{\tau}_W) \, \delta_n^2 + O(\delta_n^3) \tag{3}$$

Thus, the surface measurements of WSS using arrays of micro-pillars can provide the three-component velocity vector $\mathbf{u} = f(x, y, z = \delta n, t)$ in a wall-parallel plane at a distance of z=δn which is of order of the length of the micro-pillars. The divergence can be calculated from the sensor grid using central differences with second-order accuracy. Therefore the measurement accuracy of the wall-normal velocity component is affected by the interspacing of the micro-pillars. Assuming that the scales of the turbulence structures approaching the wall are larger than the micro-pillar interspacing and further assuming that **u** can be approximated as smooth function in space, the Taylor series truncation error of the central differencing scheme is second order. Simulations show that the measurement uncertainty in the wall-normal component is then roughly a factor of two higher than the uncertainty of the in-plane components. Thus, larger errors in the wall-normal velocity only occur if turbulences with scales smaller than the interspacing pass the array in a very short wall-normal distance. Herein, this interspacing is 500 micron, which is below the smallest scales (Kolmogorov scale) near the wall in most practical flows.

2.3 Image processing

Instead of using template matching and reference markers as done in previous processing [2], the obtained images with the wave-guiding method described herein allow using an auto-correlation procedure to obtain the components *Qx* and *Qy*. Firstly, this processing can be done for each individual pillar (variant A in Fig. 3) in small square-sized interrogation windows (IW) similar as in Particle Image Velocimetry (PIV) [1]. After subtracting the central peak in the autocorrelation map, the peak location represent the magnitude and direction of ***Q***(x,y) of the corresponding pillar, see Fig. 3. Directional ambiguity is not of a problem since the base positions of the pillars are known. A Gaussian fit at the center of the correlation peak provides a typical accuracy of order of 0.03px as computed from synthetic images. As in PIV, statistical variables can be extracted from the shape of the correlation peak if a time-series ***Q***(t) of ensembles is considered, see [8].

Another option (variant B) is to use a larger IW size that covers bundles of sensors in the array. An example is given in Fig. 3 where a subset of 3x2 sensors is used in the autocorrelation procedure. Since the array is along a regular grid with interspacing larger than the maximum tip displacement, only the center region in the autocorrelation map is sufficient to capture the

information of mean displacement and gradients. The diameter of the peak region is now broadened in the direction of shear. The peak position now represents the local average of $\boldsymbol{Q}$ and the shape of the correlation peak includes information about the spatial gradients in $\boldsymbol{Q}$. In Fig. 3B there is a strong gradient ∂Qy/∂x which stretches the peak region along the vertical axis. In addition, a non-zero gradient ∂Qx/∂x is present, too. Note that the separation of the gradients can be achieved using a rectangular IW with the long axis either in x- or in y-direction.

3. Application to an unsteady near-wall flow

The method has been applied to the flow along a plane wall of a piston crown, which is integrated in a water analogue of a 4-valve Internal Combustion (IC) engine, see Fig. 4. Further details are given in [6]. The wall is equipped with a 30×30 array of micro-pillars as documented in section 2.1. A camera mounted below the transparent piston and co-moving with the shaft records the spots shown as in Fig. 3 for an area containing 8x4 pillars. Only the inner field of 6x3 pillars could be processed for the whole cycle as some of the pillars' tips eventually leave the image borders in the highly fluctuating flow. Processing is done with the method described in variant Fig.3A for every individual pillar. The temporal evolution is recorded for the period of the intake phase in a single stroke, starting from the piston at top dead center position in quiescent conditions. Fig. 4 illustrates the experimental set-up and an exemplary result of the Q-field with strong divergence. The measurement shows the impact of the impinging jet with the piston-wall in form of source-like vector distribution of $\boldsymbol{u}_{\perp}(x, y, \partial n)$ with the center of the source in the middle of the field. In addition, the wall-normal velocity $u_n(x, y, \partial n) = u_z$ calculated from Eq. (3) is shown as a surface plot. Note that the negative z-direction of the coordinate systems is directed towards the wall, so the surface plot demonstrates a strong flow directed towards the piston wall as illustrated by the blue arrow in the sketch in Fig. 4.

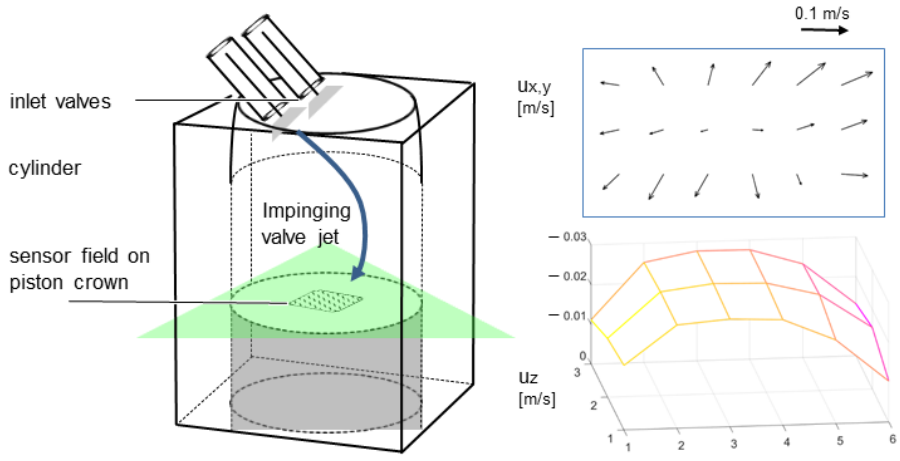

Fig. 4. Instantaneous velocity-field at a wall-normal distance of 400 micron to the piston head indicating strong wall-normal motion at a crank angle of CA=20°. The vectors indicate the tip bending relative to the pillar base on the regular grid of micro-pillars. Applying Eq. (3) reveals a strong wall-normal fluid motion towards the wall as indicated by the diverging vectors with a stagnation point near the center of the field.

The temporal evolution of wall-normal fluid motion over the whole intake cycle is given in Fig. 5 with some exemplary instants showing the flow pattern in the horizontal x,y plane. The strongest peak in uz is observed early in the intake phase at CA=20° where the valves start to

open and a jet is generated that interacts with the piston wall, compare Fig. 4. Later in the cycle, one can recognize also lift-up fluid motion which is directed away from the wall (positive uz at CA = 40°).

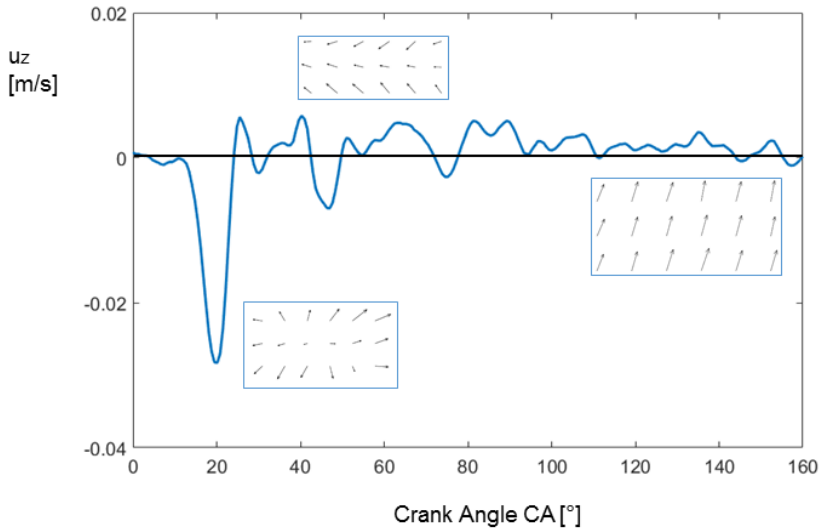

Fig. 5. Evolution of the local wall-normal velocity component uz over the intake cycle.

4. Summary and conclusion

A method is presented that uses the wave-guiding feature of flexible transparent micro-pillars in arrays to determine the near-wall flow velocity in all three components. Fluorescent labelling of the tips along a micro-pillar array is achieved by stamping. Imaging is realized from below the bottom of the transparent wall recording the light scattered from the pillar tip and guided through the pillars towards the base. As this recording also captures the light scattered from the tip in direct path to the camera, the image reveals two spots, one that corresponds to the pillar tip and the other to the base, respectively. This allows to use a 2D auto-correlation method to capture the direction and magnitude of the tip bending vector $\boldsymbol{Q}$ in the images for all individual sensors and simultaneous for a larger field of sensors. As the tip bending is proportional to the WSS it provides the WSS field along the wall. The correlation method is in principle about one order of magnitude more accurate than the precision of about 0.3px achieved with direct processing of the centroid positions of the tip spot and reference spot, which are both necessary to determine the vector $\boldsymbol{Q}$, including the measurement uncertainty of both. Maximum $|Q|$-values are of order of 50 pixel in the image plane while the minimum detectable displacement is about 1px which is limited by the fact that at very low speeds the second peak cannot be separated anymore from the central autocorrelation peak. Accuracy is further increased thanks to the fact that any influence of model or camera vibrations is cancelled out since only relative measures are taken. Processing can be done online with fast processors tuned to run the 2D autocorrelation procedure on selected sections in the images.

The method offers to calculate from the $\boldsymbol{Q}$-field the three velocity components in a plane along the tips of the pillars using the solenoidal condition in fluid mechanics for incompressible flows. For small distances from the wall of order of the length of the micro-pillars, this method can provide reasonable good estimates of the wall-normal flow close to the wall. Such a wall

e.g. can be a flat plate for fundamental studies of turbulent boundary layer flows, a curved wall of an airfoil or it could also be part of a piston head in a reciprocating engine as shown herein. In general, it is hard to achieve all three velocity components very close to the wall in flow measurements which is where the benefit of the presented method is. In addition, there is no seeding required. As all three velocity components can be captured also over ensembles in a temporal sequence, it allows to determine the statistics of the near-wall flow turbulence including the Reynolds-stresses. This information can be obtained by analyzing either the individual sensors in the field or by analyzing the shape of the correlation peak in the autocorrelation map obtained from the summation of the instantaneous maps in the sequence. A necessary precondition is that the diameter of the micro-pillars is much smaller than the smallest scales in the flow so that they don't induce disturbances on the flow itself. In addition for an interspacing larger than 20 diameters the pillars show no interference in the array. Therefore a good practical guide is to choose the limit of about 20 diameters as micro-pillar interspacing to achieve maximum spatial resolution and accuracy in all velocity components.

From a practical point of view, the subcutaneous recording can be extended by adding transmitting optics in the path towards the camera such as optical fibers. This allows then to get the information in a remote way which is currently investigated in our lab.

Acknowledgments

Funding of the position of Professor Christoph Bruecker as the BAE SYSTEMS Sir Richard Olver Chair in Aeronautical Engineering is gratefully acknowledged herein.